Triphasic scaffolds for the regeneration of the bone-ligament interface

PAPER

Triphasic scaffolds for the regeneration of the bone–ligament interface

To cite this article: G Criscenti *et al* 2016 *Biofabrication* **8** 015009

Biofabrication

PAPER

Triphasic scaffolds for the regeneration of the bone–ligament interface

G Criscenti[1,2,4], A Longoni[1,4], A Di Luca[1], C De Maria[2], C A van Blitterswijk[1,3], G Vozzi[2] and L Moroni[1,3]

[1] Department of Tissue Regeneration, MIRA Institute for Biomedical Technology and Technical Medicine, Faculty of Science and Technology, University of Twente, Enschede, The Netherlands
[2] Research center 'E. Piaggio', Faculty of Engineering, University of Pisa, Pisa, Italy
[3] Department of Complex Tissue Regeneration, MERLN Institute for Technology Inspired Regenerative Medicine, Maastricht University, Maastricht, The Netherlands
[4] These authors contributed equally to this work and share first authorship

E-mail: giu.criscenti@gmail.com

RECEIVED
25 August 2015

REVISED
8 December 2015

ACCEPTED FOR PUBLICATION
4 January 2016

PUBLISHED
29 January 2016

Keywords: electrospinning, mesenchymal stromal cells, enthesis, triphasic scaffold, interface tissue engineering

Abstract

A triphasic scaffold (TPS) for the regeneration of the bone–ligament interface was fabricated combining a 3D fiber deposited polycaprolactone structure and a polylactic co-glycolic acid electrospun. The scaffold presented a gradient of physical and mechanical properties which elicited different biological responses from human mesenchymal stem cells. Biological test were performed on the whole TPS and on scaffolds comprised of each single part of the TPS, considered as the controls. The TPS showed an increase of the metabolic activity with culturing time that seemed to be an average of the controls at each time point. The importance of differentiation media for bone and ligament regeneration was further investigated. Metabolic activity analysis on the different areas of the TPS showed a similar trend after 7 days in both differentiation media. Total alkaline phosphatase (ALP) activity analysis showed a statistically higher activity of the TPS in mineralization medium compared to the controls. A different glycosaminoglycans amount between the TPS and its controls was detected, displaying a similar trend with respect to ALP activity. Results clearly indicated that the integration of electrospinning and additive manufacturing represents a promising approach for the fabrication of scaffolds for the regeneration of tissue interfaces, such as the bone-to-ligament one, because it allows mimicking the structural environment combining different biomaterials at different scales.

1. Introduction

Tissue-to-tissue interfaces are heterogeneous zones characterized by multiple cell types and by a gradient of mechanical, structural and physico-chemical properties able to elicit a specific cell response [1]. The ligament-to-bone interface, also called 'enthesis' or 'osteoligamentous junction', plays a pivotal role in the human body facilitating synchronized joint motion, musculoskeletal function and mediating load transfer between different tissues to sustain the heterotypic cellular communications required for interface function and homeostasis [2–4]. This interface is considered a heterotypic tissue characterized by a graded structure from soft (ligament) to hard (bone) tissues with a heterogeneous distribution of cell types, matrix components and architecture [5].

Two different types of ligament-to-bone interfaces can be distinguished: fibrous (indirect) and fibrocartilaginous (direct) entheses [6]. In fibrous enthesis, Sharpey's collagen fibers connect the ligament and bone forming acute angles [7]. The fibrocartilaginous enthesis consists of a graded transition zone composed of four different tissues: fibrous connective tissue with typical fibroblasts, calcified and uncalcified fibrocartilage, and bone tissue with typical osteocytes [6]. Different hypotheses tried to explain the ligament-to-bone interface tissue healing process, which is still not completely understood. Lu *et al* suggested that tissue interface regeneration is mediated by osteoblasts and fibroblasts via heterotypic cellular interactions that may promote phenotypic changes or trans-differentiation of osteoblasts and/or fibroblasts. Furthermore, these interactions may promote the

regeneration of the fibrocartilage interface inducing the differentiation of stem cells or progenitor cells into fibrochondrocytes [3].

In the last decade, interface tissue engineering (ITE) aimed at regenerating diseased or damaged zones between different tissue types focusing its efforts on the development of engineered tissue graft able to replace the physiological function of the damaged interfaces [5, 8, 9]. Different attempts to regenerate ligament–bone interfaces are based on the use of conventional isotropic scaffolds during soft tissue reconstruction that were not integrated to bones [5], resulting in the failure of the scaffold itself [5]. Another approach is based on the design of a stratified or multi-phased biomimetic scaffolds able to reproduce the multi-tissue organization and the mechanical, structural and physicochemical graded properties present in the ligament–bone interfaces [3].

Different research groups have investigated the possibility to fabricate multiphasic or stratified scaffolds for ITE. A multiphased synthetic graft composed of 3D braided polylactic co-glycolic acid (PLGA) fibers for ACL reconstruction was proposed by Cooper *et al* [10]. The graft was composed of a femoral tunnel attachment site, a ligament region, and a tibial tunnel attachment site. In order to promote the eventual integration of the graft with bone tissue, the density of PLGA braids along the length was altered to create dense tibial and femoral sections and an open ligament region. The scaffold showed biocompatibility and acceptable mechanical properties *in vitro* and *in vivo* [10]. Another multi-region porous knitted silk ACL graft was proposed by Altman *et al* [11]. Silk fibroin, engineered to increase hydrophilicity, was incorporated into a multi-region, porous, knitted ACL graft designed to provide the necessary mechanical properties throughout bioresorption. Biological investigations demonstrated that the scaffold is biocompatible, bioresorbable, and capable of supporting cellular ingrowth and tissue remodeling. Paxton *et al* engineered functional ligament-to-bone attachment using HA and the cell adhesion RGD (Arg-Gly-Asp) peptide incorporated in a polyethylene glycol diacrylate hydrogel (PEGDA) [12]. The incorporation of HA into PEGDA hydrogels reduced the swelling ratio but increased mechanical strength and stiffness of the hydrogels and the capacity for cell growth and interface formation. Further increasing the proportion of HA into PEG hydrogels improved interface formation, but with high levels of HA the PEG-HA composite became brittle. An opposite trend was detected with the RGD incorporation. Combining HA and RGD, better cell attachment was obtained; however, no differences in mechanical properties than PEG alone were detected. In addition, Ma *et al* fabricated a bone–ligament–bone structure introducing specific bone segments to ligament monolayers. In particular, the monolayers were rolled up around the bone pieces and self-assembled into a ligament–bone–ligament construct [4, 13]. Spalazzi *et al* proposed a stratified triphasic scaffold (TPS) for the regeneration of ACL-to-bone interface composed by three continuous phases [14, 15]. A polymer fiber knitted mesh was used to mimic the ligament region, polymer microspheres for fibrocartilage and sintered polymer ceramic composite microspheres for bone tissues [14]. The scaffold promoted cell proliferation and phenotypic matrix production. Sahoo *et al* proposed a biodegradable nano-microfibrous polymer scaffold by electrospinning PLGA nanofibers onto a knitted PLGA scaffold in order to provide a large biomimetic surface for cell attachment [16]. This scaffold facilitated cell seeding and promoted cell proliferation, function, and differentiation.

These results demonstrated that a stratified approach could be an adequate alternative for the fabrication of structure for bone–ligament interface regeneration. However, gradient scaffolds with continuous transition in composition and mechanical properties were proposed as alternative to the previous approach due to the possibility to obtain a smoother integration of the different tissue types [4, 5]. Singh *et al* proposed a 3D multiphased PLGA microsphere scaffold with a continuous stiffness gradient obtained by incorporating calcium carbonate or titanium dioxide into the microspheres [17]. A linear gradient of calcium phosphate, which induced a mechanical gradient on the structure, was created on gelatin-coated polycaprolactone (PCL) nanofibers by Li *et al* [18]. These studies showed that the multi-material approach to design stratified or multi-phased biomimetic scaffold and the possibility to tailor its mechanical properties represent suitable alternatives to reproduce the multi-tissue organization present in the ligament–bone interfaces. However, the design of a multiphased scaffold able to mimic the micro- and nano-scale gradients present at the bone–ligament interface represents a challenge for ITE.

In this study, a 3D fiber deposited–electrospun (3DF–ESP) TPS for the regeneration of the bone–ligament interface was proposed. Using structural features as leading criteria to mimic the bone–ligament interface, a scaffold with a linear gradient of materials, mechanical and structural properties was fabricated combining ESP and 3DF techniques. PCL and PLGA were selected for the electrospinning and 3DF processes, respectively. PCL is commonly used for bone tissue engineering, while PLGA is a well-known bioresorbable polymer with potential applications for ligament repair [19–25].

2. Materials and methods

2.1. Scaffold fabrication

Scaffolds were fabricated through a two-step process (figure 1). Initially, PCL (average Mn ~45 000, Sigma

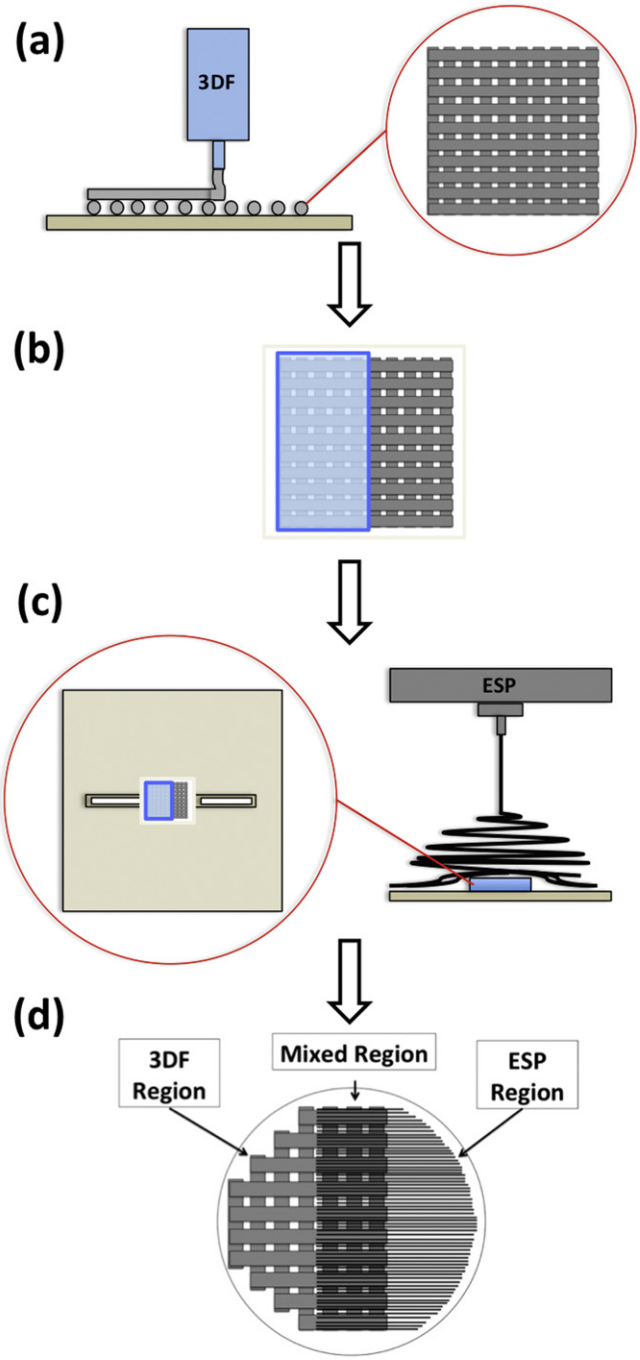

Figure 1. Two-step fabrication process: (a) PCL 3DF scaffolds with 0–90 layer configuration and with 90° orientation between successive layers were manufactured with a Bioscaffolder device; (b) subsequently, the PCL 3DF scaffolds were partially covered with a paper foil and used as a target for the ESP jet; (c) an aligned PLGA ESP fibrous network was fabricated on top of the uncovered portion of the 3DF scaffolds; (d) finally, the paper foil was removed and triphasic scaffolds with 3DF, ESP and mixed regions were obtained.

Aldrich, The Netherlands) 3DF scaffolds were manufactured with a Bioscaffolder device (SysENG, Germany). The polymer was put in a stainless steel syringe and heated at $T = 100\,^{\circ}\mathrm{C}$ for 30 min. A nitrogen pressure of 5 Bars was applied to the syringe through a pressurized cap when the molten phase was achieved. The fiber diameter d_1, the fiber spacing d_2, the layer thickness d_3 and the number of deposited layers were set at 250 μm (inner diameter of the nozzle used for plotting), 700 μm, 150 μm and 4, respectively. The scaffold architecture was determined by a 0–90 layer configuration where fibers were deposited with 90° orientation steps between successive layers. The plotting speed was maintained within 275–325 mm min^{-1}.

Subsequently, the PCL 3DF scaffold was partially covered (two thirds of its surface) with a paper foil, fixed on a PDMS surface and used as a target for the ESP jet. In order to have an aligned fiber network, the sample was positioned on a modified collector composed by two flat electrodes and used as a target for the ESP jet (figure 1).

An aligned ESP fibrous network was fabricated from a 4% (w/v) PLGA 85:15 solution in 1, 1, 1, 3, 3, 3-hexafluoro-2-propanol (HFIP) on top of the uncovered portion of the 3DF scaffold. The voltage was 20 kV, the air gap was 20 cm and the flow rate was 1 ml h^{-1}. Electrospinning was performed in an environmental chamber with a controlled temperature of 25 °C and a relative humidity of 30%. The polymer solution was loaded into a 5 ml syringe (BD Biosciences) and pumped using a syringe pump (KDS-100-CE, KD Scientific) through a Teflon tube connected to a stainless steel needle (0.5 mm inner diameter, 0.8 mm outer diameter). The needle was mounted in a 30 × 20 cm upper parallel plate and centered on the custom made collector. The ESP fiber density was determined as the time frame used during fabrication, which was set to 90 min. At the end of this two-step process, the paper foil and the fibers on top of it were removed with a scalpel and a scaffold with 3 different regions was obtained.

2.2. Scaffold characterization

2.2.1. Geometry and architecture

Scaffolds morphology, geometry and architecture were characterized by scanning electron microscopy (SEM) analysis (XL 30 ESEM-FEG, Philips). Before the observations, the samples were gold sputtered (Cressington Sputter Coater 108 auto) and the fiber diameter, fiber spacing, and layer thickness were evaluated from SEM pictures measuring 100 fibers using FIJI image analysis software.

2.2.2. Porosity

The porosity of 3DF region was calculated following the theoretical approach by Landers *et al* [26] (equation (1)):

$$P_{\text{th}} = 1 - V_{\text{scaffold}}/V_{\text{cube}} = 1 - \frac{\pi}{4} \cdot \frac{d_1^2}{d_2 \cdot d_3}, \quad (1)$$

where P_{th} is the theoretical scaffold porosity, d_1 the fiber diameter, d_2 the fiber spacing and d_3 the layer thickness.

The porosity of ESP and mixed regions was experimentally measured by measuring the ratio between the apparent density of the scaffold and the specific density of the bulk material (equation (2)):

$$P_{\text{exp}} = 1 - \rho_{\text{struct}}/\rho = 1 - \frac{M}{V} \cdot \frac{1}{\rho}, \quad (2)$$

where P_{exp} is the scaffold porosity, ρ is the specific density of the polymers ($\rho_{\text{PLGA 85:15}} = 1.2825$ g cm^{-3} and $\rho_{\text{PCL}} = 1.145$ g cm^{-3}), and M and V are the measured mass and volume of the scaffold.

The porosity of the mixed region was evaluated considering the volume fractions of the different materials (equation (3)):

$$P_{\text{mix}} = P_{\text{esp}} \cdot f_{\text{esp}} + P_{\text{3DF}} \cdot f_{\text{3DF}}, \quad (3)$$

where P_{mix}, P_{esp} and P_{3DF} are the porosities of the mixed, electrospun and 3DF regions and while f_{esp} and f_{3DF} are the volume fractions of the electrospun and 3D printed parts of the mixed region, respectively (equations (4) and (5)):

$$f_{\text{esp}} = \frac{V_{\text{3DF}}}{V_{\text{esp}} + V_{\text{3DF}}}, \quad (4)$$

$$f_{\text{esp}} = \frac{V_{\text{esp}}}{V_{\text{esp}} + V_{\text{3DF}}}, \quad (5)$$

where V_{3DF} and V_{esp} are the volume of the 3DF and electrospun parts of the mixed region respectively.

2.2.3. Mechanical properties analysis: uniaxial tensile test

Uniaxial tensile tests were performed to evaluate the tensile mechanical properties of each region of the TPS. A total of six samples per region were tested in dry condition. The samples were rectangular shaped with surgical scalpel so that the length-to-width aspect ratio (4:1) provided uniform tensile stress in the region where the strain was measured. All the samples had a constant cross-sectional area (CSA), as measured with a digital calliper (accuracy of 0.02 mm and resolution of 0.01 mm). The samples were fixed in standard clamps and axially aligned to the 500 N load cell of a Zwick Z020 material-testing machine.

The scaffolds were preconditioned by a series of ten cycles, to 3% of strain at a strain rate of 0.1% s^{-1}, in order to reduce hysteresis. The samples were then tested to failure at a strain rate of 0.3% s^{-1}. With CSA and strain measurements, a stress–strain curve representing the tensile mechanical properties of the different regions was created. From the stress–strain curves, the following parameters were obtained: Young's modulus (MPa), defined as the slope of the linear region of the stress–strain curve, ultimate stress (MPa), ultimate strain (%) and strain energy density (MPa) at failure. The failure mode was also noted.

2.3. Biological investigations

The biological investigations were performed both in the single parts (partition analysis) and on the entire structure (total analysis). In the first case, after the cell culture the three different areas of the TPS (3DF, mixed and ESP) were divided using a cutter and analysed separately in order to have a better understanding of how cellular behavior is affected by the single regions. The rationale related to the partition analysis is based on the hypothesis to use the three different regions (3DF, mixed and ESP) to regenerate three different tissue types (bone, fibrocartilagineous region and ligament, respectively). In order to verify this hypothesis, the different regions were cultured in basic, mineralization, and ligament media to cover the possible *in vitro* scenarios, including controls. In the second case, the entire TPS was analysed to evaluate how it performs compared to the controls. The rationale related to the full analysis is based on the hypothesis that the TPS performs better than its

controls (FDM, ESP and mixed regions). The full analysis was performed using different media because there is no evidence in literature of a specific medium for a co-colture able to promote the various type of differentiation.

In both cases the controls were represented by scaffolds composed by only a single region, thus being only eletrospun, 3DF and mixed structures. For the alkaline phosphatase (ALP) activity and glycosaminoglycans (GAG) amount evaluations, the total analysis was performed considering that the ALP and GAG total values were obtained from the arithmetical addition of the single region values.

GAG and ALP activity analysis were performed after 7 days in proliferation medium (PM) and other 7 days in differentiation medium. The rationale related to the choice of these time points is based on the evaluation of the triphasic architecture influence on early differentiation.

2.3.1. Cell culture

Colony-picked human mesenchymal stem cells (hMSCs) (male, age 22) were retrieved from the Institute of Regenerative Medicine (Temple, Texas) [27]. Briefly, a bone marrow aspirate was drawn and mononuclear cells were separated using density centrifugation. Cells were plated in order to obtain adherent hMSCs, which were harvested once they reached 60%–80% of confluence (passage 0). The hMSCs were expanded, harvested and frozen at passage 1 (P1) for distribution. The P2 cells were expanded at initial seeding density of about 1000 cells cm^{-2} in PM which consists of alpha minimum essential medium (MEM-α, Gibco) supplemented with L-glutamine (2 mM, Gibco), penicillin (100 U ml^{-1}, Gibco), streptomycin (100 μg ml^{-1}, Gibco), FBS (10% (w/v), Lonza), ascorbic acid (0.2 mM, Sigma) and basic fibroblast growth factor (1 ng ml^{-1}, bFGF, Instruchemie). The hMSCs were harvested at approximately 80% of confluence for seeding on TPSs.

Before the sterilization procedure, scaffolds were placed in a sterile non-treated 12-well plate (NUNC). Viton® polymer rings (Eriks b.v., The Netherlands), with an outer diameter of 22 mm and inner diameter of 19.6 mm, were sterilized in 70% ethanol and inserted into the well to hold scaffolds to the bottom. The scaffolds were then sterilized in 70% ethanol for 15 min, subsequently washed twice in PBS for 5 min and finally incubated in PM overnight to pre-wet the scaffold and promote protein adsorption. Before the seeding procedure, scaffolds were dried. The harvested P3 hMCSs were seeded on TPSs and controls with a density of 140 000 cells cm^{-2} (500 000 cells/scaffold) in 1.5 ml of PM. The media were refreshed every 2–3 days until day 7 in order to have almost a constant cell distribution and density at the beginning of every experiment. After seven days of culture, the medium was changed to the differentiation media (mineralization medium (MM) and ligament medium (LM)) and the control one basic medium (BM). Cells were grown at 37 °C in a humidified atmosphere with 5% CO_2.

For this study four different types of media were used. BM was used after cell seeding on the scaffolds as control for mineralization and ligament media. BM consisted of alpha minimum essential medium (α-MEM, Gibco) supplemented with L-glutamine (2 mM, Gibco), penicillin (100 U ml^{-1}, Gibco) and streptomycin (100 μg ml^{-1}, Gibco), FBS (10% (w/v), Lonza) and ascorbic acid (0.2 mM, Sigma). The MM, used for cell differentiation toward the osteogenic lineage, consisted of BM containing 10 nM dexamethasone (Sigma) and 0.01 M β-glycerophosphate (BGP, Sigma). The LM, used for cell differentiation into tenocytes and fibroblasts, was BM with the supplement of 10 ng ml^{-1} of transforming growth factor beta 3 (TGF-β3, R&D Systems). During cell expansion and for seven days after seeding, PM was used. The composition was the same of the BM with the supplement of basic fibroblast growth factor (1 ng ml^{-1}, bFGF, Instruchemie).

2.3.2. Scanning electron microscopy (SEM)

After 3 days, cell attachment and distribution were observed using a Philips XL ESEM-FEG. Briefly, scaffolds were rinsed twice with PBS and fixed in 10% formalin for 15 min. Subsequently, the samples were dehydrated in sequential ethanol series (50%, 60%, 70%, 80%, 90%, 96% and 100%), 15 min for each concentration. For the final dehydration step, scaffolds were immersed in hexamethyldisilazane (Sigma-Aldrich) and the solvent was left to evaporate overnight. Finally samples were gold sputter-coated (Cressington Sputter Coater 108 auto) prior to study them under the SEM [28, 29]. SEM images were obtained under high vacuum with an acceleration voltage of 10 kV and a working distance of 10 mm.

2.3.3. Presto blue assay

Presto blue assay (Life technology) was performed to evaluate cell viability, proliferation and metabolic activity after 1, 5 and 7 days of culture. Briefly, the cell permeable resazurin-based solution provided was diluted ten times in the same type of medium in which cells were cultured, according to the manufacturer's instructions. 700 μl of BM supplemented with presto blue reagent were added to each plate and incubated for two hours in the dark at 37 °C in a humidified atmosphere with 5% CO_2. The reducing power of living cells modified the reagent, which turned red in color and became highly fluorescent. From each sample, 100 μl of medium were transferred in a clear bottom black 96 well plate and the color change was detected using a spectrophotometer LS50B (Victor 3, Perkin Elmer) according to the manufacturer's instructions (excitation/emission maxima: 535–560/

590–615 nm). The experiments were performed in triplicates.

2.3.4. DNA assay

In order to quantify the cell number, the amount of DNA was calculated with CyQuant DNA assay kit (Molecular Probes, Invitrogen) after 7 days of culture, according to the manufacturer's description. Briefly, samples were stored at −30 °C and freeze-thawed 5 times. Afterwards, the constructs were digested for 16 h at 56 °C with 1 mg ml^{-1} proteinase K (Sigma Aldrich) in Tris/EDTA buffer (pH 7.6). The solution is composed of 18.5 μg ml^{-1} of iodoacetamine (Sigma Aldrich) and 1 μg ml^{-1} pepstatin A (Sigma Aldrich). To avoid the interference caused by the binding of the dye to the RNA, 100 μl of the sample were incubated for one hour at room temperature with 100 μl of lysis buffer provided by the kit (component B diluted in 180 mM NaCl, 1 mM EDTA in distilled water in the ratio 1:20) in which RNAse enzyme was diluted 1000 times. Quantification of the total DNA was performed using a green fluorescent dye provided by the kit (excitation 480 nm, emission 520 nm). Fluorescence was measured at 480 nm using a spectrophotometer LS50B (Victor 3, Perkin Elmer) and DNA concentrations were calculated from a λ DNA standard curve.

2.3.5. ALP assay

A partition and total ALP analysis were performed. The TPSs and their controls were cut and stored at −30 °C. After the thawing steps, the samples were incubated for one hour at room temperature in a cell lysis buffer composed of 0.1 M KH_2PO_4, 0.1 M K_2HPO_4 and 0.1% Triton X-100 (Acros Chemicals), pH 7.8. ALP activity quantification was performed using a CDP-Star kit (Roche), according to manufacturer's protocol. Briefly, 40 μl of CDP-Star reagent were added to 10 μl of cell lysate. After 15 min of incubation at room temperature in the dark, chemoluminescence was measured at 420 nm with a spectrophotometer LS50B (Victor 3, Perkin Elmer). The obtained values were normalized to the DNA amount per sample.

2.3.6. GAG assay

The amount of GAG was determined spectrophotometrically after reaction with 16 mg of dimethylmethylene blue dye (DMMB, Sigma-Aldrich) in a 10 mM hydrochloric acid solution containing 3.04 g l^{-1} of glycine and 2.37 g l^{-1} of NaCl (pH 3). A micro plate reader (Multiskan GO, Thermo Fisher) was used to determine the absorbance at 525 nm. The amount of GAG was calculated using a standard of chondroitin sulphate (Sigma-Aldrich). The GAG production was normalized to DNA quantity per sample.

2.3.7. Fluorescent staining

A fluorescence analysis was performed to evaluate cell morphology and distribution after 3 days of culture. Briefly, scaffolds were rinsed twice with PBS and fixed in 10% formalin for 15 min. Cell membranes were permeabilised with 0.25% (v/v) Triton X-100 (Sigma-Aldrich) in PBS for 5 min, followed by rinsing in PBS three times for 5 min. Nonspecific binding was blocked using 1% (w/v) BSA in PBS. Nuclei were labeled incubating the samples with 100 ng ml^{-1} of 4', 6' diamidin-2'-phenylindoldihydrochlorid (DAPI, in PBS, Sigma, Munich, Germany) for 20 min. After rinsing the sample 3 times with PBS, to visualize the cytoskeleton, actin filaments were stained with 200 ng ml^{-1} of phalloidin (Alexa Fluor 594 phalloidin, Invitrogen) for 1 h. Samples were rinsed 3 times, stored in the dark and subsequently analysed on a fluorescent microscope (Nikon Eclipse E600). For DAPI staining, a BFP filter (excitation wavelength 379–401 nm, emission wavelength 438–485) and for phalloidin, a Texas Red filter (excitation wavelength 542–576 nm, emission wavelength 600–675 nm) were used. Pictures were taken with a Nikon DS-Fi1c camera equipped with NIS-Element software.

2.4. Statistical analysis

All data are expressed as mean ± standard deviation. Biochemical assays were performed with triplicate biological samples. A one-way statistical analysis of variance (ANOVA) with a significant level p of 0.05 was used to determine differences among the groups. A two-way ANOVA with a significant level p of 0.05 was used to determine differences among the group and different time points. In both cases, Tukey's multiple comparisons test was used to perform post hoc analysis. Statistical significance between the control group and the experimental groups are indicated with (*) which represents a p-value < 0.05, (**) which represents a p-value < 0.01, and (***) which represents a p-value < 0.001.

3. Results

3.1. Scaffold structure and architecture

The TPSs were characterized by three different regions: the 3DF, the ESP and the mixed parts (figure 2). The scaffold had a circular shape and a surface of 3.5 mm^2 equally divided among the three regions.

SEM analysis revealed a fiber diameter of 208 ± 7.1 μm, a fiber spacing of 734 ± 15 μm, and a layer thickness of 202 ± 9 μm for the 3DF region (figure 2(a)). The fiber diameter of the ESP network was 0.588 ± 0.02 μm (figures 2(b) and (c)). This corresponded to a porosity of 77.1 ± 1.7% for the 3DF region, and to a porosity of 95.9 ± 1.6% for the ESP one. The porosity of the mixed region was measured as 80.2 ± 2.7%. The scaffolds presented interconnected porous structures and no layer delamination phenomenon occurred.

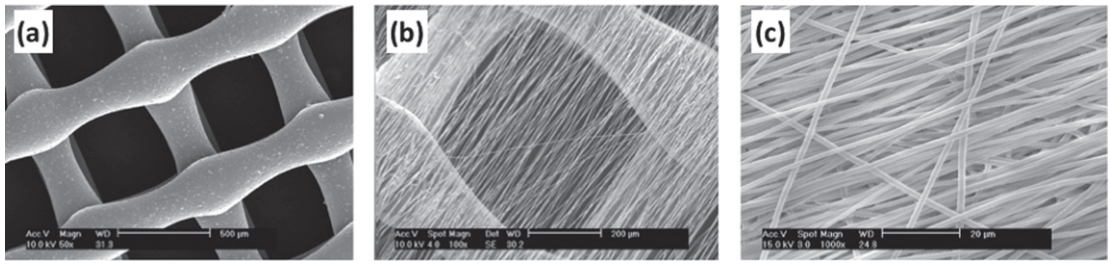

Figure 2. Triphasic scaffold regions: (a) 3DF region (scale bar: 500 μm), (b) mixed region (scale bar: 200 μm), (c) ESP region (scale bar: 20 μm).

Table 1. Mechanical properties of the three different regions.

Material properties	3DF	Mixed	ESP
Ultimate stress (MPa)	1.62 ± 0.27	2.57 ± 0.51	5.21 ± 1.11
Ultimate strain (%)	4.81 ± 0.69	6.71 ± 0.31	22.1 ± 3.2
Young's modulus (MPa)	43.6 ± 8.1	50.6 ± 10.5	88.9 ± 15.1
Strain energy density (MPa)	1.78 ± 0.27	1.81 ± 0.39	2.14 ± 0.81

3.2. Mechanical analysis

The mechanical behavior of the different regions of the TPSs was evaluated performing uniaxial tensile tests. During the preconditioning phase, the three regions showed hysteresis phenomena. During the uniaxial tensile testing phase, stress–strain curves representing the mechanical properties of the structure were obtained. All the samples failed at the middle region ($n = 6$), indicating that the tensile test was appropriately set up. The obtained results are listed in table 1 and figure 3.

The three regions showed a different mechanical behavior. The Young's modulus of the ESP region was statistically higher than the modulus of the 3DF region. For the mixed region, it seems that the 3DF part was predominant and influenced the tensile mechanical behavior of the entire scaffold (figure 3(a)).

Similar trends were found for the ultimate stress and ultimate strain (figures 3(b) and (c)). No statistical differences were found for the strain energy density (figure 3(d)). These results demonstrated that the TPS is characterized by a gradient of mechanical properties that could stimulate different cell response and differentiation.

3.3. Cell morphology and distribution

Cell morphology and distribution after 3 days of culture in PM were evaluated through SEM and fluorescence analysis (figure 4). These analyses revealed that hMSCs were homogeneously distributed on the entire scaffold and at the interface areas. In the ESP mesh they are well spread, whereas on the 3DF region they connect the fibers by bridging the pores. No cell clusters due to the cell seeding were observed.

3.4. Cell proliferation and metabolic activity

The metabolic activity after 1, 5 and 7 days in PM was evaluated with Presto blue assay (figure 5(a)). All the samples showed an increase of metabolic activity except for the control of the mixed region. The TPS showed a metabolic activity that seemed to be an average of the controls at each time point. After 7 days in proliferation media the study was carried on using two different media for the differentiation analysis (MM and LM) while BM was used as a control. The metabolic activity of the different regions of the TPS was evaluated after 7 days in differentiation media. The partition analysis on the different areas of the TPSs showed a similar trend after 7 days in differentiation medium (figure 5(b)).

In all the media, the ESP region showed the highest metabolic activity. When comparing the three media, BM supported a higher metabolic activity in all the regions.

After 14 days of culture (7 d in PM and 7 d in BM/MM/LM) a partition and a total DNA assay were performed. Total DNA analysis (figure 6(a)) showed no statistical differences among the different culture conditions. However, statistically different behaviors were found between the TPS and its controls. In particular, the TPSs showed a higher number of cells compared to mixed control in BM and MM while a similar trend was detected with 3DF control in LM.

For the partition analysis, figure 6(b) shows that no statistical differences in the cell number were found comparing the different regions of the TPS and there were no differences among the different culture conditions.

3.5. Evaluation of ALP activity analysis

ALP is an enzyme responsible for the dephosphorylation of several molecules including nucleotides and proteins. ALP has always been related to osteoblast differentiation, as an increase of the enzyme activity was observed in the early stages of their commitment [30]. After 7 days in PM and 7 days in MM, hMSCs

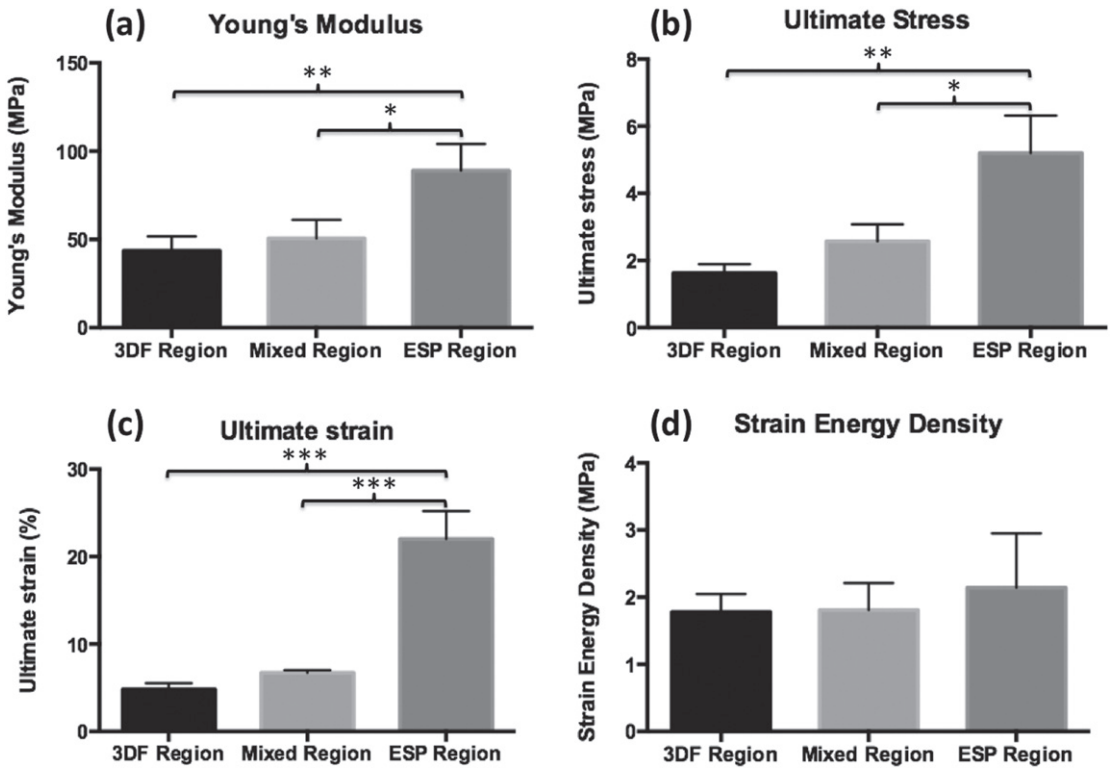

Figure 3. Mechanical properties of the different regions.

differentiation was studied evaluating ALP activity both on partitioned and bulk scaffold samples.

Observing the total ALP activity, the entire TPS showed a statistically higher ALP activity in MM compared to the three different controls (figure 7(a)). Considering the two media, statistically higher ALP activities (p-value < 0.001) were found in all the different regions when MM was used. The increase in ALP activity along the entire culture period could represent a first indication of hMSCs differentiation toward the osteogenic lineage.

Comparing the different areas of the TPS after 7 days in differentiation medium, it is possible to identify a trend in ALP activity in case of MM (figure 7(b)). ALP seemed higher in the 3DF part, suggesting a possible differentiation toward the osteogenic lineage, whereas it decreased in the mixed and in the ESP regions. Considering the two media, statistically higher ALP activities (p-value < 0.001) were found in all the different parts when MM was used.

3.6. GAG analysis

GAGs secretion was determined as an indicator for ligamentogenesis. After 7 days in PM and 7 days in LM, hMSCs differentiation was studied evaluating GAG content and performing partition and total GAG Assays. Observing the total GAGs amount, the entire TPS showed a statistically higher GAG content in BM and LM compared to the three different controls (figure 8(a)).

Despite no statistical differences were found among the different regions of the TPSs after 7 days in LM (figure 8(b)), the different GAG amount among the TPS and its controls, in addition to a similar trend in ALP activity, suggested that the triphasic configuration seems to influence hMSCs behavior *in vitro*.

4. Discussion

Engineering interface tissues requests a complex strategy that includes the use of specific biomaterials and fabrication techniques to recreate the adequate multi-tissue transition, but also specific cell types and culture conditions to promote growth and differentiation.

A successful scaffold for ITE applications has minimum requirements in terms of biological, biochemical and physical properties [31]. Materials should have adequate mechanical properties to resist to wound contraction forces invoked during tissue healing *in vivo*. In addition, sufficient structural integrity is fundamental to obtain stable mechanical conditions and vascularization of the host site [31, 32].

In this study, a biomimetic approach was used to design a 3DF–ESP TPS for the regeneration of the bone–ligament interface. PCL and PLGA based scaffolds with a graded variation of their physico-chemical and mechanical properties were fabricated in a two-step process to mimic the multi-tissue

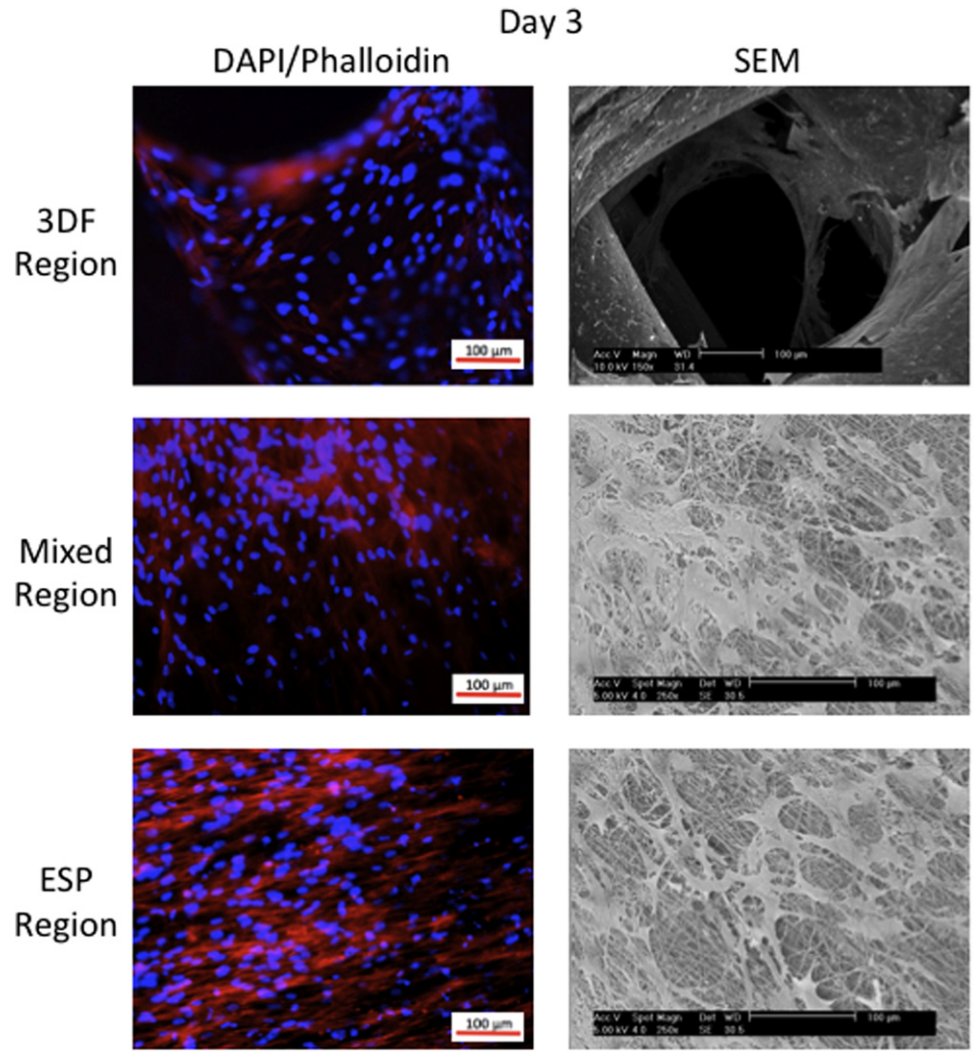

Figure 4. Cell morphology and distribution after 3 days of culture.

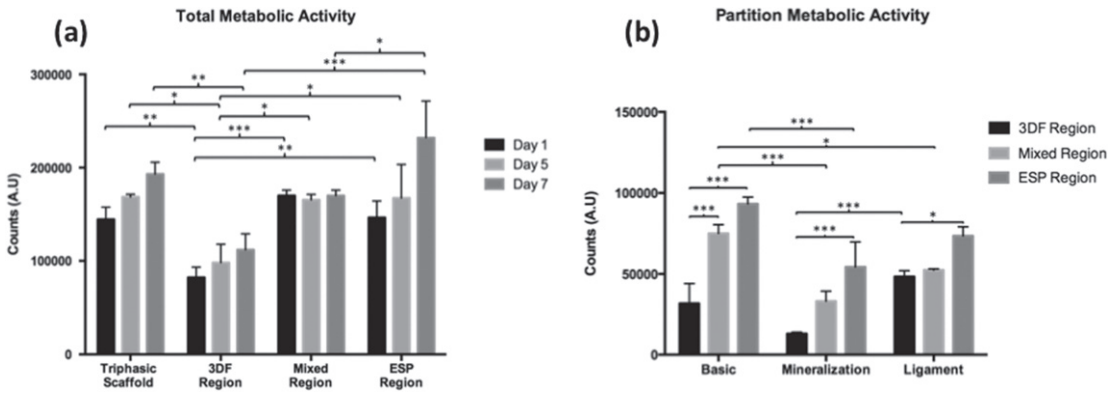

Figure 5. (a) Metabolic activity after 1, 5 and 7 days in PM: triphasic scaffold showed a metabolic activity that seemed to be an average of the controls at each time point. Controls were represented by scaffolds composed by only one region, thus being only electrospun, 3DF and mixed structures; (b) partition metabolic activity after 7 days in PM and other 7 days in BM/MM/LM in the different control scaffolds. Controls were represented by scaffolds composed by only one region, thus being only eletrospun, 3DF and mixed structures.

organization of the native ligament-to-bone insertion site. Electrospinning of PLGA was used to mimic the ligament, tissue while the bone tissue was reproduced by 3D fiber deposition of PCL. The fibrocartilagineous region was reproduced combining the previous techniques. The presence of different regions could support different cell type and favor the formation of different tissues on a single construct.

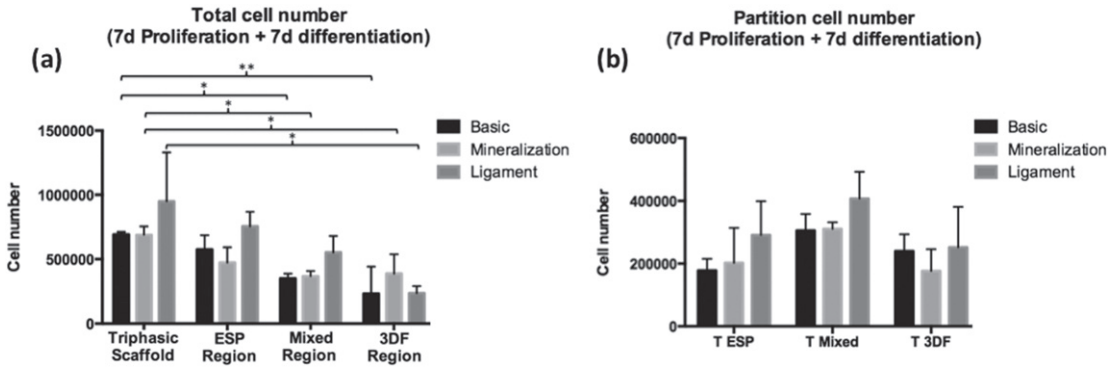

Figure 6. (a) Total cell number after 7 days in PM and other 7 days in BM/MM/LM. Controls were represented by scaffolds composed by only one region, thus being only eletrospun, 3DF and mixed structures; (b) partition cell number after 7 days in PM and other 7 days in BM/MM/LM.

The use of different biomaterials processed by two different techniques allowed the fabrication of scaffolds with interconnected porous regions and with different morphologies and porosities. Assembling the different phases of the scaffold represented a difficult step of the fabrication process. Several authors proposed different methods. Moroni *et al* directly electrospun fibers on top of the FDM structure, where FDM and electrospinning were alternatively carried out in a layer-by-layer process [33]. In this way, the ESP network was blocked between two layers of FDM structures. Vaquette *et al* tried to quickly immerse the bottom part of an FDM scaffold into a specific solvent producing a severe damage in the ESP structure [31]. For this reason, a heat press-fitting treatment was utilized for the adhesion of ESP fiber on the FDM construct [31]. Park *et al* used a solid free form fabrication technique combined with multiple polymers casting process to fabricate PCL/PGA hybrid constructs [34]. In our case, the choice of specific polymers, solvent and techniques, as well as the optimization of fabrication and environmental parameters, allowed to fabricate a TPS by directly electrospinning on top of the FDM structure without the use of additional steps. This phenomenon is probably due to the HFIP vapor that promoted the fiber welding to the 3DF structure. The porosity analysis of the 3DF–ESP TPS revealed values within the range of natural bone tissue for the 3DF region and within the range of the ligament tissue for the ESP region [35].

The concept of designing structures with continuous or step-wise change in micro- and macrostructure and in the resulting physico-chemical and mechanical properties has about two decades of history. The use of gradient or stratified structures for ITE applications, for example, could optimize the implant capability of withstanding different mechanical loads at specific regions minimizing stress-shielding [36]. Stratified multiphased scaffolds have been investigated for orthopaedic TE and in particular for osteochondral applications [14].

Mechanical analysis of the TPS demonstrated that its different regions have different tensile mechanical properties and its mechanical gradient could stimulate different cell response. A similar result was obtained by Li *et al* who generated a linear gradient of calcium phosphates on a non-woven mat of electrospun nanofibers, which influenced the mechanical behavior of the structure [18]. Observing the mechanical results, the ESP region showed a higher Young's modulus compared to the 3DF ones. This is probably due to the presence of large pores on the 3DF structure that reduced the effective CSA while the much more tightly packed ESP regions had the effective CSA closer to the apparent one. Observing the mixed part, two different sub-regions can be easily identified: the ESP and 3DF structures. Both regions, during uniaxial tensile test, were subjected to the same deformation. For this reason, in first approximation, the mechanical behavior of the mixed region can be homogenized using a Voigt model consisting of two springs in parallel. In this case the mechanical response is described by the equation (6):

$$E_{\text{tot}} = \upsilon_{\text{Esp}} \cdot E_{\text{Esp}} + \upsilon_{\text{3DF}} \cdot E_{\text{3DF}}, \tag{6}$$

where E_{tot} is the Young's modulus of the entire structure, υ_{Esp} and υ_{3DF} are the volume fractions of the ESP and 3DF sub-regions while E_{Esp} and E_{3DF} represent the Young's moduli of the ESP and 3DF regions.

The different thicknesses and, consequently, the different cross sectional areas influenced the volume fractions and the effective contribution of each subregion to the Young's modulus of the mixed part. For this reason, despite $E_{\text{3DF}} < E_{\text{Esp}}$, $\upsilon_{\text{Esp}} \ll \upsilon_{\text{3DF}}$ and the 3DF part is predominant and influence the tensile mechanical behavior of the entire mixed region.

Nevertheless, Matyas *et al* quantified the principal stresses as function of spatial position in the femoral insertion of medial collateral ligament [37]. They demonstrated that the resultant of the principal stresses is a two-dimensional vector: the principal tensile stresses were identified in the ligament substance and

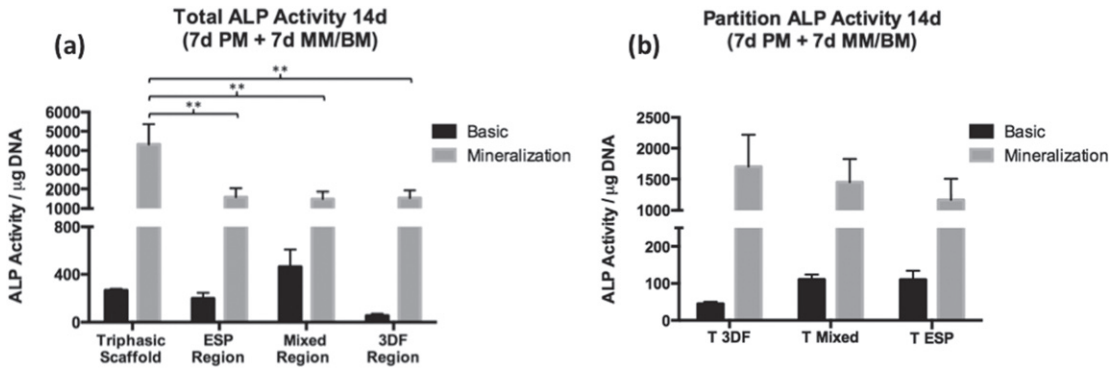

Figure 7. (a) Total ALP activity after 7 days in PM and other 7 days in BM/MM. Controls were represented by scaffolds composed by only one region, thus being only eletrospun, 3DF and mixed structures; (b) partition ALP activity after 7 days in PM and other 7 days in BM/MM.

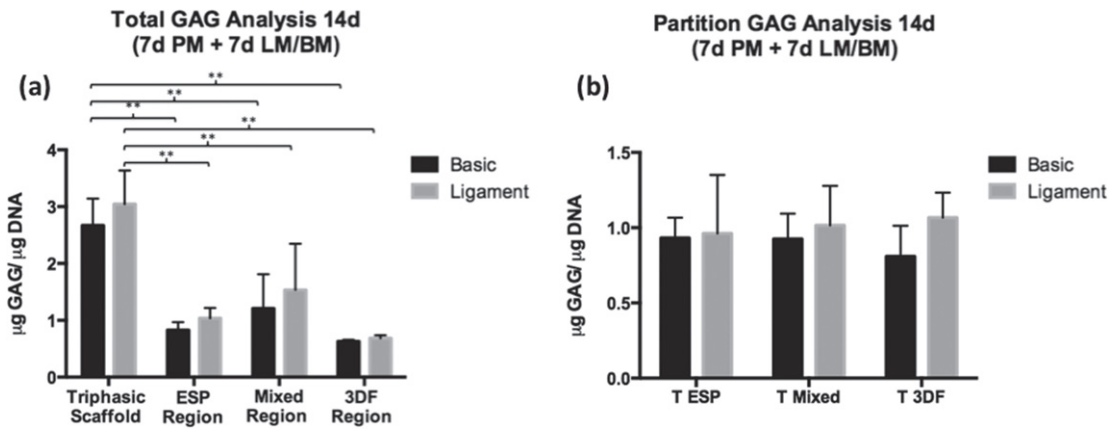

Figure 8. (a) Total GAGs after 7 days in PM and other 7 days in BM/LM. Controls were represented by scaffolds composed by only one region, thus being only electrospun, 3DF and mixed structures; (b) partition GAGs after 7 days in PM and other 7 days in BM/LM.

followed the collagen fiber orientation while a combination of tensile and compressive stresses were identified along the inner curvature of the insertion near the hard–soft-tissue interface. These results suggested that compressive tests should be performed as well to better understanding the mechanical behavior of scaffolds. However, during uniaxial compression test, the ESP and 3DF sub-regions of the mixed part would be subjected to the same stress. For this reason, in first approximation, the mechanical behavior of the mixed region could be homogenized using a Reuss model consisting of two springs in series. In this case the mechanical response is described by equation (7):

$$E_{\text{tot}} = \frac{E_{3\text{DF}} \cdot E_{\text{Esp}}}{\upsilon_{\text{Esp}} \cdot E_{3\text{DF}} + \upsilon_{3\text{DF}} \cdot E_{\text{Esp}}}. \qquad (7)$$

From equation (7), it is possible to conclude that, the total Young's modulus is strongly dependent from the volume fractions. In particular, $\upsilon_{\text{Esp}} \ll \upsilon_{3\text{DF}}$ and the $E_{\text{tot}} \approx E_{3\text{DF}}$. The compressive elastic modulus of the 3DF region is similar to the tensile one [38]. For this reason, in the case of the mixed region only tensile tests were performed.

As hMSCs are an easily available cell source at the implantation site in orthopaedic applications, seeding these cells on such TPSs and evaluating their activity could be a valid analysis to check the scaffold ability to induce a specific response related to the specific region. Cell seeding efficiency on 3DF, ESP and mixed scaffold was previously evaluated [33, 39, 40]. Cell morphology and distribution analysis on the 3DF–ESP TPSs revealed that hMSCs were homogeneously distributed on the entire scaffold and at the interface areas. The graded structural and mechanical properties also influenced the metabolic activity of the TPS. Moreover, the presence of a mechanical gradient could contribute hMSCs differentiation toward the osteogenic, chondrogenic and ligamentogenic lineages, although previous studies focusing on the influence of Young's modulus on stem cell differentiation used hydrogels of significantly lower stiffness compared to the scaffolds here developed [41]. This scenario seems to be supported by the ALP activity results. Even though ALP is highly expressed by cells in mineralized tissue, its function is not completely understood. It appears to act as a promoter of the mineralization process both increasing the local

concentration of inorganic phosphate and decreasing the concentration of extracellular pyrophosphate [42]. As consequence, it is possible to assume that an upregulation in ALP activity reflects the number of osteogenic committed progenitor cells in a population. However, high variations in both ALP levels and *in vitro* induction kinetics were observed between hMSCs from different donors [43]. The higher ALP activity showed by the TPS compared to the controls in the total analysis and the increase in ALP activity along the different regions represented a first indication of hMSCs differentiation toward the osteogenic lineage. This analysis suggested that the 3DF region of the TPS could support early bone formation. GAGs analysis revealed higher GAG content in the TPS compared to the controls and no significant differences among the different regions. This behavior could also be due to the early time points used for GAGs analysis. Typically, GAGs are synthesized at later time points and future investigations will evaluate the GAGs amount after 2 weeks of culture in differentiation medium.

The design of a multiphased structure composed of an FDM scaffold (bone compartment) and an electrospun membrane (ligament compartment) was also proposed by Vaquette *et al* to regenerate the periodontal ligament (PDL) [31]. Using a cell-based strategy, osteoblasts culture and multiple PDL cell sheets were combined to achieve bone and PDL regeneration. *In vitro* studies demonstrated that osteoblasts produced mineralized matrix in the bone compartment and the PDL cell sheet harvesting did not induced significant cell death [31]. *In vivo* studies confirmed *in vitro* analysis showing an intense ALP staining in the bone compartment with osteoblasts culture and the incorporation of the multiple PDL cell sheets. However, also in this case, all the biological investigations were carried out using two different primary cell types. The approach proposed in our study to engineer the bone–ligament interface is based on the use of two materials with different mechanical properties and permitted the fabrication of a scaffold with a three different graded zones. The main advantage of this approach is the possibility to create a structure that closely mimic the structural, mechanical and topographical properties at the micro- and nano-scale of the bone, ligament, and calcified/uncalcified fibrocartilagineous regions, simultaneously.

The use of stratified and multiphase scaffolds for ITE has been previously described in other studies [15, 44]. However, to the best of our knowledge, in literature there are studies related to only stratified scaffold or only multiphased ones. For this reason, the 3DF–ESP TPS can be considered the first example of the simultaneous combination of stratified and multi phased approaches on two different spatial directions, due to its phase variation along its length (3DF, mix, ESP) and to the stratification along the thickness showed in the mixed region.

The 3DF–ESP TPS can represent an *in vitro* model of the ligament-to-bone interface. In order to develop a fully integrated interface scaffold, future investigations will focus on cell–cell (osteoblast–fibroblasts) [45] and cell–scaffold interactions (e. g. effect on preservation of cellular phenotype, effect on the release of mediators such as chemotactic and growth factors that elicit and sustain inflammatory responses at the implant site) and on corroborating these initial indications suggesting an influence of the proposed scaffold design on hMSCs differentiation through gene expression analysis of specific osteogenic and ligamentogenic markers, as well as analysis of functional protein markers (e.g. mineralization for bone, collagen type I formation for ligament) at later time points. Moreover, an osteoblasts–fibroblasts co-culture can be performed to analyse the phase-specific cell distribution and heterogeneity during long term culture.

5. Conclusions

Interface tissue regeneration requires a coordinated response of the different soft- and hard-tissues during the wound healing process [31]. ITE is an emerging field and the proposed 3DF–ESP TPS represents a possible and viable alternative for the regeneration of bone-to-ligament interface promoting bone formation and ligament regeneration. The integration of ESP and 3DF represents a promising technique for the manufacturing of interface scaffolds able to come a step closer in mimicking the structural biological environment through the combination of different biomaterials at different scales.

Acknoledgements

We would like to acknowledge Dr Paul Wieringa for its precious suggestion for the Electrospinning experimental setup.

References

[1] Phillips J E, Burns K L, Le Doux J M, Guldberg R E and García A J 2008 Engineering graded tissue interfaces *Proc. Natl Acad. Sci. USA* **105** 12170–5
[2] Benjamin M, Evans E J and Copp L 1986 The histology of tendon attachments to bone in man *J. Anat.* **149** 89–100
[3] Lu H H and Jiang J 2006 Interface tissue engineering and the formulation of multiple-tissue systems *Adv. Biochem. Eng. Biotechnol.* **102** 91–111
[4] Lu H H, Subramony S D, Boushell M K and Zhang X 2010 Tissue engineering strategies for the regeneration of orthopedic interfaces *Ann. Biomed. Eng.* **38** 2142–54
[5] Seidi A, Ramalingam M, Elloumi-Hannachi I, Ostrovidov S and Khademhosseini A 2011 Gradient biomaterials for soft-to-hard interface tissue engineering *Acta Biomater.* **7** 1441–51
[6] Hammoudi T M and Temenoff J S 2011 Biomaterials for regeneration of Tendons and Ligaments *Biomaterials for Tissue Engineering Applications* ed J A Burdick and R L Mauck (Vienna: Springer) pp 307–41

[7] Yang P J and Temenoff J S 2009 Engineering orthopedic tissue interfaces *Tissue Eng.* B **15** 127–41
[8] Sahoo S, Teh T K, He P, Toh S L and Goh J C 2011 Interface tissue engineering: next phase in musculoskeletal tissue repair *Ann. Acad. Med. Singap.* **40** 245–51
[9] Moffat K L, Wang I-N E, Rodeo S A and Lu H H 2009 Orthopedic interface tissue engineering for the biological fixation of soft tissue grafts *Clin. Sports Med.* **28** 157–76
[10] Cooper J A, Lu H H, Ko F K, Freeman J W and Laurencin C T 2005 Fiber-based tissue-engineered scaffold for ligament replacement: design considerations and in vitro evaluation *Biomaterials* **26** 1523–32
[11] Altman G H, Horan R L, Weitzel P and Richmond J C 2008 The use of long-term bioresorbable scaffolds for anterior cruciate ligament repair *J. Am. Acad. Orthop. Surg.* **16** 177–87
[12] Paxton J Z, Donnelly K, Keatch R P and Baar K 2009 Engineering the bone–ligament interface using polyethylene glycol diacrylate incorporated with hydroxyapatite *Tissue Eng.* A **15** 1201–9
[13] Ma J, Goble K, Smietana M, Kostrominova T, Larkin L and Arruda E M 2009 Morphological and functional characteristics of three-dimensional engineered bone–ligament–bone constructs following implantation *J. Biomech. Eng.* **131** 101017
[14] Spalazzi J P, Doty S B, Moffat K L, Levine W N and Lu H H 2006 Development of controlled matrix heterogeneity on a triphasic scaffold for orthopedic interface tissue engineering *Tissue Eng.* **12** 3497–508
[15] Spalazzi J P, Dagher E, Doty S B, Guo X E, Rodeo S A and Lu H H 2008 *In vivo* evaluation of a multiphased scaffold designed for orthopaedic interface tissue engineering and soft tissue-to-bone integration *J. Biomed. Mater. Res.* A **86** 1–12
[16] Sahoo S, Ouyang H, Goh J C-H, Tay T E and Toh S L 2006 Characterization of a novel polymeric scaffold for potential application in tendon/ligament tissue engineering *Tissue Eng.* **12** 91–9
[17] Singh M, Sandhu B, Scurto A, Berkland C and Detamore M S 2010 Microsphere-based scaffolds for cartilage tissue engineering: using subcritical CO(2) as a sintering agent *Acta Biomater.* **6** 137–43
[18] Li X, Xie J, Lipner J, Yuan X, Thomopoulos S and Xia Y 2009 Nanofiber scaffolds with gradations in mineral content for mimicking the tendon-to-bone insertion site *Nano Lett.* **9** 2763–8
[19] Williams J M, Adewunmi A, Schek R M, Flanagan C L, Krebsbach P H, Feinberg S E, Hollister S J and Das S 2005 Bone tissue engineering using polycaprolactone scaffolds fabricated via selective laser sintering *Biomaterials* **26** 4817–27
[20] Sobral J M, Caridade S G, Sousa R A, Mano J F and Reis R L 2011 Three-dimensional plotted scaffolds with controlled pore size gradients: effect of scaffold geometry on mechanical performance and cell seeding efficiency *Acta Biomater.* **7** 1009–18
[21] Li X *et al* 2014 3D-printed biopolymers for tissue engineering application *Int. J. Polym. Sci.* **2014** 829145
[22] Lu H H, Cooper J A, Manuel S, Freeman J W, Attawia M A, Ko F K and Laurencin C T 2005 Anterior cruciate ligament regeneration using braided biodegradable scaffolds: *in vitro* optimization studies *Biomaterials* **26** 4805–16
[23] Chen G, Sato T, Sakane M, Ohgushi H, Ushida T, Tanaka J and Tateishi T 2004 Application of PLGA-collagen hybrid mesh for three-dimensional culture of canine anterior cruciate ligament cells *Mater. Sci. Eng.* C **24** 861–6
[24] Sahoo S, Ang L-T, Cho-Hong Goh J and Toh S-L 2010 Bioactive nanofibers for fibroblastic differentiation of mesenchymal precursor cells for ligament/tendon tissue engineering applications *Differentiation* **79** 102–10
[25] Yilgor C, Yilgor Huri P and Huri G 2012 Tissue engineering strategies in ligament regeneration *Stem Cells Int.* **2012** 374–676
[26] Landers R, Pfister A, Hübner U, John H, Schmelzeisen R and Mülhaupt R 2002 Fabrication of soft tissue engineering scaffolds by means of rapid prototyping techniques *J. Mater. Sci.* **37** 3107–16
[27] Digirolamo C M, Stokes D, Colter D, Phinney D G, Class R and Prockop D J 1999 Propagation and senescence of human marrow stromal cells in culture: a simple colony-forming assay identifies samples with the greatest potential to propagate and differentiate *Br. J. Haematol.* **107** 275–81
[28] Fontana G, Srivastava A, Thomas D, Lalor P, Dockery P and Pandit A 2015 Three-dimensional microgel platform for the production of cell factories tailored for the nucleus pulposus *Bioconjug. Chem.* **26** 1297–306
[29] Browne S, Fontana G, Rodriguez B J and Pandit A 2012 A protective extracellular matrix-based gene delivery reservoir fabricated by electrostatic charge manipulation *Mol. Pharm.* **9** 3099–106
[30] Siffert R S 1951 The role of alkaline phosphatase in osteogenesis *J. Exp. Med.* **93** 415–26
[31] Vaquette C, Fan W, Xiao Y, Hamlet S, Hutmacher D W and Ivanovski S 2012 A biphasic scaffold design combined with cell sheet technology for simultaneous regeneration of alveolar bone/periodontal ligament complex *Biomaterials* **33** 5560–73
[32] Woodruff M A and Hutmacher D W 2010 The return of a forgotten polymer–polycaprolactone in the 21st century *Prog. Polym. Sci.* **35** 1217–56
[33] Moroni L, Schotel R, Hamann D, de Wijn J R and van Blitterswijk C A 2008 3D fiber-deposited electrospun integrated scaffolds enhance cartilage tissue formation *Adv. Funct. Mater.* **18** 53–60
[34] Park C H, Rios H F, Jin Q, Bland M E, Flanagan C L, Hollister S J and Giannobile W V 2010 Biomimetic hybrid scaffolds for engineering human tooth–ligament interfaces *Biomaterials* **31** 5945–52
[35] Sikavitsas V I, Temenoff J S and Mikos A G 2001 Biomaterials and bone mechanotransduction *Biomaterials* **22** 2581–93
[36] Miao X and Sun D 2010 Graded/gradient porous biomaterials *Materials* **3** 26–47
[37] Matyas J R, Anton M G, Shrive N G and Frank C B 1995 Stress governs tissue phenotype at the femoral insertion of the rabbit MCL *J. Biomech.* **28** 147–57
[38] Hutmacher D W, Schantz T, Zein I, Ng K W, Teoh S H and Tan K C 2001 Mechanical properties and cell cultural response of polycaprolactone scaffolds designed and fabricated via fused deposition modeling *J. Biomed. Mater. Res.* **55** 203–16
[39] Leferink A M, Hendrikson W J, Rouwkema J, Karperien M, van Blitterswijk C A and Moroni L 2013 Increased cell seeding efficiency in bioplotted three-dimensional PEOT/PBT scaffolds *J. Tissue Eng. Regen. Med.* (doi:10.1002/term.1842)
[40] Leferink A M, Santos D, Karperien M, Truckenmüller R K, van Blitterswijk C A and Moroni L 2015 Differentiation capacity and maintenance of differentiated phenotypes of human mesenchymal stromal cells cultured on two distinct types of 3D polymeric scaffolds *Integr. Biol.* **7** 1574–86
[41] Engler A J, Sen S, Sweeney H L and Discher D E 2006 Matrix elasticity directs stem cell lineage specification *Cell* **126** 677–89
[42] Golub E E and Boesze-Battaglia K 2007 The role of alkaline phosphatase in mineralization *Curr. Opin. Orthopaedics* **18** 444–8
[43] Prins H-J, Braat A K, Gawlitta D, Dhert W J A, Egan D A, Tijssen-Slump E, Yuan H, Coffer P J, Rozemuller H and Martens A C 2014 In vitro induction of alkaline phosphatase levels predicts *in vivo* bone forming capacity of human bone marrow stromal cells *Stem Cell Res.* **12** 428–40
[44] He P, Sahoo S, Ng K S, Chen K, Toh S L and Goh J C H 2013 Enhanced osteoinductivity and osteoconductivity through hydroxyapatite coating of silk-based tissue-engineered ligament scaffold *J. Biomed. Mater. Res.* A **101** 555–66
[45] Wang I-N E, Shan J, Choi R, Oh S, Kepler C K, Chen F H and Lu H H 2007 Role of osteoblast–fibroblast interactions in the formation of the ligament-to-bone interface *J. Orthop. Res.* **25** 1609–20